INFERRING AVALANCHE DYNAMICS AND MAGNITUDE FROM INFRASOUND SOURCE LOCATION AND ENERGY PROXY

Ulivieri G. [1], Ripepe M.[2], Lacanna G.[2], Biagioli F.[2], Chen D.[3], Dreier L.[3], Steinkogler W.[3], Magnan D.[4]

[1] GECO s.r.l., Florence, Italy
[2] University of Florence, Florence, Italy
[3] Wyssen Avalanche Control, Revelstoke, BC, Canada
[4] Parks Canada, Mt Revelstoke and Glacier National Park, BC, Canada

ABSTRACT: Infrasound is nowadays routinely used for avalanche detection, but its potential to constrain avalanche dynamics and magnitude remains poorly quantified. We investigated this capability within the Avalanche Detection Network (ADN) at Rogers Pass, British Columbia, using two IDA® systems with direct line of sight to avalanche paths. Dual-array back-azimuth triangulation was used to track the dominant coherent infrasonic source during avalanche propagation. The localised source migrated from the release area toward the deposition zone, consistent with a runout of 1504 m and a mean source-centroid speed of 24.7 m/s. Independent Doppler radar (LARA) observations give a comparable runout of 1518 m and a mean speed of 20.5 m/s. The time-dependent 3-D source-to-array distance was then used to correct the recorded infrasonic amplitude for first-order geometrical spreading and to define the Infrasonic Avalanche Energy proxy (IAVE). IAVE is calculated as the time integral of the Hilbert envelope of the distance-corrected infrasonic pressure. Analysis of 27 avalanches shows that IAVE increases systematically across independently assigned Parks Size classes at both arrays. Empirical regressions of $\log_{10}$(IAVE) against the numerical Parks Size classes yield nearly identical slopes at the two IDA® systems (0.934 and 0.939) and R^2 values of 0.971 and 0.995, respectively. This near-unit scaling is noteworthy because successive whole classes of the Canadian avalanche Size scale themselves correspond approximately to order-of-magnitude increases in characteristic avalanche mass and destructive potential. Localisation-related uncertainty is small compared with the observed within-class variability, with median 95% relative uncertainties of 0.41% and 0.26%. These results indicate that multi-array infrasound can retrieve first-order avalanche dynamics and suggest that IAVE may provide an empirical proxy for avalanche magnitude. Further validation across the larger ADN catalogue is required to assess the influence of avalanche flow dynamics, source-generation mechanisms, terrain, and propagation conditions.

KEYWORDS: Infrasonic Detection of Avalanches IDA®, avalanche dynamics, infrasonic avalanche energy proxy.

1. INTRODUCTION

Infrasound monitoring has become an established tool for the automatic detection and remote observation of snow avalanches, particularly in mountainous areas where direct visual observations are often limited (Ulivieri et al., 2011; Hendrikx et al., 2018; Mayer et al., 2020). In recent years, increasingly dense infrasonic networks and multi-array processing techniques have also demonstrated the potential to retrieve information on the location and propagation of avalanche-generated signals. However, the characterization of avalanche infrasound sources and the relationships between infrasonic signals, avalanche dynamics, and avalanche magnitude remain only partially explored (Johnson et al., 2021; Sovilla et al., 2025).

The Avalanche Detection Network (ADN) has operated at Rogers Pass, British Columbia, since 2019 to support Parks Canada avalanche forecasting and mitigation activities (Hendrikx et al., 2018). The network includes multiple infrasonic arrays (IDA®) monitoring 121 avalanche paths and has recorded thousands of avalanche signals since 2018. Within the network, a sector monitored simultaneously by two infrasonic arrays and by an independent Doppler radar (LARA) provides particularly favourable conditions for investigating the physical meaning of the infrasonic observations.

Here, we first explore whether multi-array infrasound can track the motion of the dominant acoustic source during an avalanche and provide first-order estimates of dynamic parameters such as runout and mean propagation velocity. Source

Giacomo Ulvieri, GECO S.R.L.,
Via Salaiola 59, 50053 Empoli – Firenze (Italy);
tel: +39 3289715345;
email: giacomo@geco-company.com

https://doi.org/10.15788/1790099214

localization is then used to account for the changing source-to-array distance and derive a distance-corrected, time-integrated infrasonic source-strength proxy. The main objective of this exploratory study is to test whether this infrasonic proxy systematically increases with independently assigned Parks avalanche Size and can therefore provide a basis for remotely estimating avalanche magnitude.

2. INFRASONIC SOURCE LOCATION

Estimating an infrasonic source-strength proxy requires knowledge of the source-to-receiver distance. Source localization is therefore a prerequisite for removing the first-order effect of geometrical spreading from the recorded signal.

In this exploratory study, we focused on a sector of the Rogers Pass network with a comparatively simple source–receiver geometry (Fig. 1).

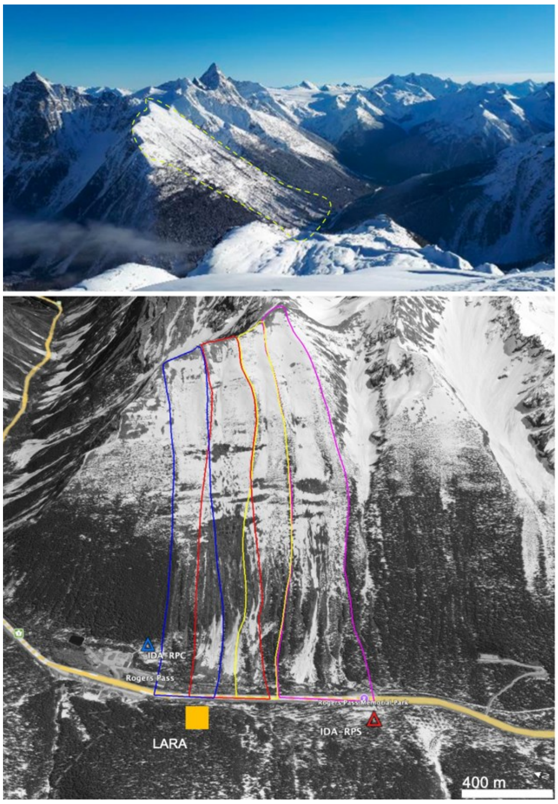

Figure 1: Study site and instrumental configuration at Rogers Pass, British Columbia, Canada. Top: view of the monitored avalanche sector (dashed outline). Bottom: Google Earth of selected avalanche paths with position of IDA® (RPC and RPS) and LARA Doppler radar.

The two IDA systems (RPC and RPS) have line of sight to four adjacent avalanche paths located at < 2.5 km distance, which are characterized by broadly planar slopes and limited lateral confinement. This configuration was selected to minimize, at first order, uncertainties associated with topographic shielding and terrain-controlled acoustic propagation, thereby providing favourable conditions for infrasonic source localization and subsequent source–receiver distance correction.

The infrasonic source was localised by triangulating back-azimuth (*bkz*, source direction) estimates obtained independently at the two IDA systems (Fig. 2a, RPC and RPS) using array cross-correlation analysis (e.g., Ulivieri et al., 2011). Back-azimuth detections were aggregated over 1-s intervals using the median *bkz* value and detection time (Fig. 2b). RPC and RPS back-azimuth estimates within a ±8-s window were paired, and source positions were calculated by intersecting the corresponding back-azimuth rays. Pair consistency was evaluated from the mismatch between the observed inter-array delay and that predicted from the corresponding source-to-array range difference, assuming an effective acoustic celerity of 330 m/s (pairs with a residual ≤1.2 s were retained). No constraint to a predefined avalanche path was imposed.

Source elevations were subsequently derived from the digital elevation model (DEM) and combined with the plan-view localisations to derive 3-D source-to-array distances and the cumulative 3-D path coordinate of the localised source centroid as well as the trend of the source propagation velocity (Fig. 2c). Within-bin *bkz* variability was propagated through the triangulation to quantify localisation uncertainty. For the example shown in Fig. 2, median *bkz* variability was 0.18° at RPC and 0.14° at RPS, corresponding to a median 95% source-position uncertainty of approximately 12 m and relative source-distance uncertainties of approximately 1.0% and 0.6%, respectively.

The localised infrasonic source, as expected, progressively migrated downslope (Path 61) from the release area toward the deposition zone, indicating that the dominant coherent infrasonic radiation was associated with a source moving down-hill.

The dynamic parameters retrieved from infrasonic source localisation were evaluated against independent LARA Doppler radar measurements (Fig. 3). For the example event, the 3-D runout estimate from infrasound (1504 m) shows close agreement with the LARA estimate (1518 m), while the average 3-D source-centroid speed derived from infrasound is moderately higher than the radar estimate (24.7 versus 20.5 m/s; Tab. 1).

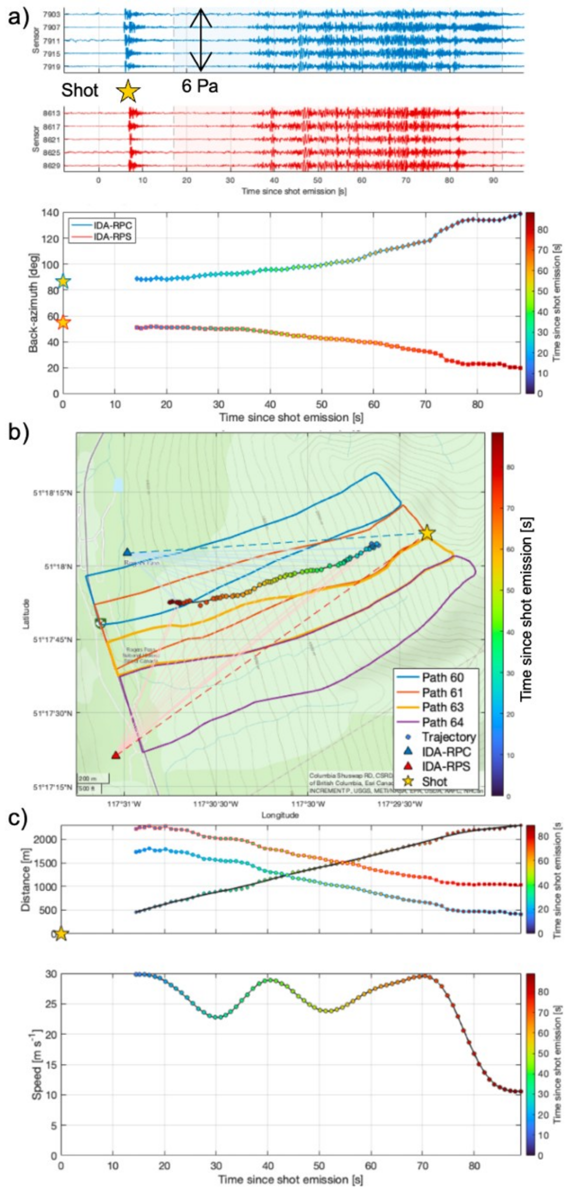

Figure 2: Example of dual-array infrasonic localisation and source-dynamics retrieval for avalanche 23 in Tab. 2. a) Infrasonic waveforms and corresponding back-azimuth at the two IDA systems. b) Map of the infrasonic-derived source locations. c) Temporal evolution of the 3-D source-to-array distances and cumulative 3-D source-centroid path coordinate and corresponding 3-D source-centroid speed.

The infrasonic source should not be interpreted as a specific physical point within the avalanche or directly as the position of the avalanche front; rather, it represents the position of the dominant coherent infrasonic source. Nevertheless, the downslope migration and the agreement with independent radar-derived dynamic parameters indicate that the dominant infrasonic source is dynamically coupled to the moving avalanche.

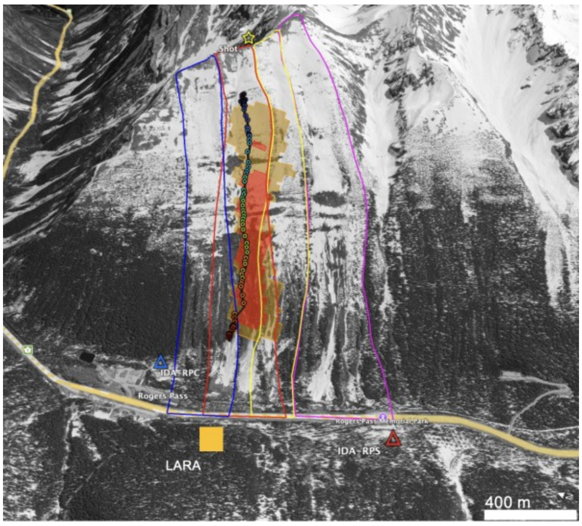

Figure 3: Google Earth view of the comparison between the infrasonic source trajectory (coloured circles) and the LARA radar measurements for avalanche 23 in Tab. 2. Coloured circles indicate successive infrasonic source locations, while the shaded area represents the radar-detected avalanche extent.

Table 1: Comparison of infrasound- and radar-derived avalanche dynamic parameters.

Parameter	***Infrasound IDA®***	***Radar LARA***
3D runout distance [m]	1504	1518
Average speed [m/s]	24.7	20.5

We thus used the time-dependent source position to correct the recorded infrasonic amplitudes for the source-to-array distance.

3. INFRASONIC AVALANCHE ENERGY PROXY

From the 2021–2026 Parks Canada catalogue, we considered only avalanches occurring within the selected paths that were detected by both IDA systems, had an assigned Parks avalanche Size, and a reliable observation time (timeInterval = 0), allowing unambiguous association with the corresponding infrasonic signals. The final dataset includes 27 avalanches ranging from Size 2 to 4 (Tab. 2). Among events with a known release type, all but one were slab avalanches. Avalanches below Size 2.5 are under-represented, likely reflecting the reduced detectability of small events given the IDA-ADN geometry.

Parks Size follows the Canadian avalanche size classification, which assigns five classes according to avalanche destructive potential (McClung and Schaerer, 1981; Canadian Avalanche Association, 2024).

Table 2: Parks Canada avalanche observations used in the IAVE analysis. Na, natural avalanche; Xa, artillery-triggered avalanche; Xh, Heli bombing. CAASC: Canadian Avalanche Association avalanche size scale. RelDesc: avalanche release type.

Event	Trigger	Observation date [PDT]	Path	RelDesc
1	Xa	2022-04-04 08:56	061	Slab
2	Xa	2024-02-29 01:11	060	Slab
3	Xa	2025-02-01 01:20	060	Slab
4	Xa	2022-12-25 10:26	064	Slab
5	Xa	2023-04-10 08:09	061	Unknown
6	Xh	2023-04-30 16:36	064	Unknown
7	Na	2024-01-29 12:13	061	Slab
8	Xa	2024-02-25 15:21	061	Slab
9	Na	2024-03-11 19:40	061	Slab
10	Na	2025-03-26 05:49	060	Unknown
11	Xa	2022-01-17 18:33	061	Slab
12	Xa	2022-01-17 18:35	061	Slab
13	Xa	2022-03-01 19:22	064	Slab
14	Na	2024-03-17 17:35	061	Loose
15	Xa	2025-12-10 19:21	064	Slab
16	Xa	2025-12-15 13:53	061	Slab
17	Xa	2025-12-15 13:58	063	Slab
18	Xa	2026-02-28 00:57	063	Slab
19	Xa	2026-02-28 00:59	064	Slab
20	Xa	2026-03-08 05:24	063	Slab
21	Xa	2022-01-17 18:37	064	Slab
22	Na	2023-04-30 14:43	064	Unknown
23	**Xh**	**2023-04-30 17:03**	**061**	**Unknown**
24	Xh	2023-04-30 17:09	063	Unknown
25	Xh	2023-05-04 14:11	064	Slab
26	Xa	2026-03-18 07:05	064	Slab
27	Na	2026-03-18 22:41	061	Slab

Destructive potential depends on avalanche mass, speed and density, as well as on path geometry, and successive whole Size classes correspond approximately to order-of-magnitude increases in characteristic avalanche mass. Parks Size is therefore treated here as an ordinal reference variable rather than as a direct quantitative measurement of avalanche mass, volume or kinetic energy.

For each event, the infrasonic waveform was band-pass filtered between 0.8 and 10 Hz. Source elevations were obtained from a digital elevation model and combined with the infrasonic localisation to calculate the time-dependent 3-D source-to-array distance.

Assuming *1/r* geometrical spreading, we define the Infrasonic Avalanche Energy proxy (IAVE, eq. 1 and eq. 2) as the time integral of the envelope of the distance-corrected infrasonic pressure:

$$P_{corr}(\mathrm{t}) = \mathrm{p(t)} \cdot r(t) \quad (1)$$

$$IAVE = \int_{t_0}^{t_1} \sqrt{P_{corr}(t)^2 + [H\{P_{corr}(t)\}]^2}\, dt \quad (2)$$

where *p(t)* is the band-pass-filtered recorded infrasonic pressure, *r(t)* is the time-dependent 3-D source-to-array distance, and *H* denotes the Hilbert transform. IAVE is expressed in Pa m s (Fig. 4).

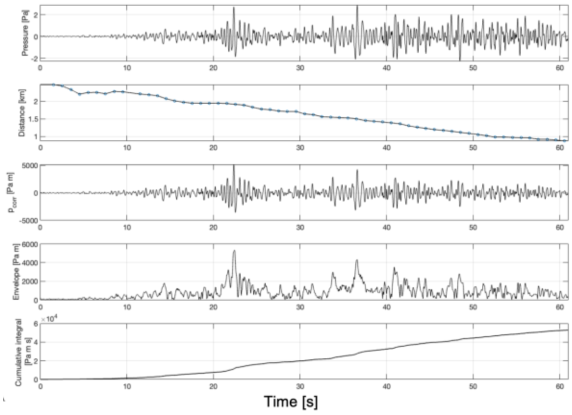

Figure 4: Example calculation of the Infrasonic Avalanche Energy proxy (IAVE) for avalanche E083. From top to bottom: band-pass-filtered infrasonic pressure, time-dependent 3-D source-to-array distance, distance-corrected pressure, Hilbert envelope, and cumulative IAVE.

We do not assume here a direct conversion between the measured IAVE and avalanche mass or kinetic energy. Instead, we test the simpler working hypothesis that larger avalanches, involving a larger and/or longer-lived dynamically active source, produce a greater time-integrated infrasonic source strength.

Events were grouped according to their independently assigned Parks Size, and the median IAVE and the first and third quartiles (25^{th} and 75^{th} percentiles, respectively) were calculated separately for RPC and RPS (Fig. 5). To quantify the empirical IAVE–Size relationship, the Size-class median IAVE values were fitted separately for RPC and RPS by linear regression of $\log_{10}$(IAVE) against the numerical Parks Size classes,

$$log_{10}(IAVE) = a \cdot S + b \quad (3)$$

where *S* denotes Parks Size. The regressions were therefore performed on the Size-class median values rather than on the individual avalanche observations. The resulting coefficients, with IAVE expressed in Pa m s, are a=0.934 and b=0.924 for RPC, and a=0.939 and b=0.983 for RPS, with R^2=0.971 and 0.995, respectively.

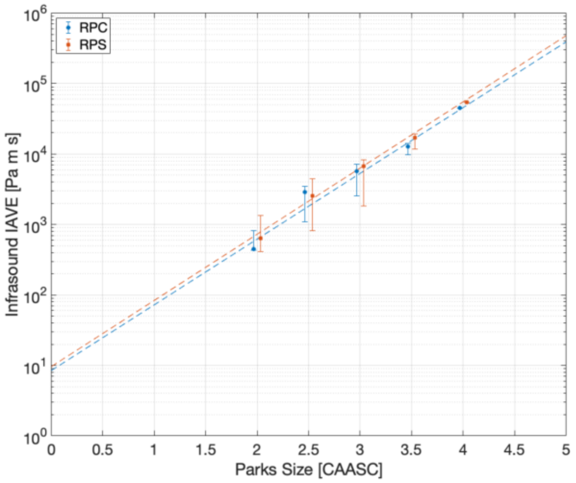

Figure 5: Relationship between Infrasonic Avalanche Energy proxy (IAVE) and Parks avalanche Size (CAASC). Symbols indicate Size-class median IAVE values, while vertical bars span the first to third quartile (25th and 75th percentiles, respectively), representing the central 50% of the observations within each Size class. Dashed lines show the regressions of the Size-class median values in logarithmic space for RPC and RPS.

Despite the limited number of events and the variability within individual Size classes, the median IAVE increases systematically with Parks Size at both IDAs. In particular, the nearly identical regression slopes obtained independently at RPC and RPS (0.934 and 0.939, respectively) indicate a remarkably consistent empirical scaling relationship between IAVE and Parks Size at the two arrays.

The near-unit slopes in log-IAVE space are noteworthy because the Canadian avalanche Size scale itself is approximately logarithmic in terms of characteristic avalanche mass and destructive potential (McClung and Schaerer, 1981; Canadian Avalanche Association, 2024), although Size is not treated here as a direct physical measure of avalanche mass or energy.

Propagation of within-bin *bkz* variability showed that localization-related uncertainty has only a minor effect on IAVE, with median 95% relative uncertainties of 0.41% at RPC and 0.26% at RPS, substantially smaller than the observed within-class variability. Part of this variability is inherently associated with comparing a continuous infrasonic quantity with the discrete and ordinal Parks Size classification, whereby avalanches of different physical magnitude may be grouped within the same Size class; additional variability may arise from the observer-based Size estimation itself (Hafner et al., 2023). Potentially more important, differences in avalanche flow dynamics and in the efficiency of infrasonic source generation may account for a substantial fraction of the observed scatter.

Finally, the close agreement between the RPC and RPS scaling relationships, despite the different source–receiver geometries of the two arrays, strongly supports the interpretation of IAVE as an event-scale property of the avalanche-generated infrasonic source rather than a residual effect of source distance alone.

4. CONCLUSION

This preliminary analysis indicates that infrasound can provide information on avalanche dynamics beyond event detection alone. The progressive downslope migration of the localized infrasonic source from the release area toward the deposition zone indicates that the dominant coherent infrasonic radiation is dynamically coupled to the moving avalanche. The close agreement between infrasonic and radar estimates of runout, together with the comparable estimates of mean propagation velocity, further indicates that the motion of the acoustic source centroid captures first-order characteristics of avalanche dynamics.

The time-integrated Infrasonic Avalanche Energy proxy (IAVE) increases systematically with independently assigned Parks avalanche Size, despite substantial event-to-event variability within individual Size classes. Localization-related uncertainty has only a minor influence on IAVE, with median 95% relative uncertainties of 0.41% at RPC and 0.26% at RPS, much smaller than the observed within-class variability. Potentially more important, differences in avalanche flow dynamics and infrasonic source-generation efficiency may contribute substantially to the observed scatter, although these effects cannot yet be quantified. The comparable Size dependence independently observed at RPC and RPS is particularly encouraging.

These preliminary results support the use of infrasound not only for avalanche detection and localization, but also as a potential proxy for avalanche magnitude. If confirmed on a larger and more diverse dataset, the approach could ultimately enable near-real-time estimates of avalanche Size directly from an operational infrasonic monitoring network, including events occurring under poor visibility or where dedicated radar observations are unavailable.

Several limitations remain. The physical mechanism responsible for the dominant infrasonic radiation is not yet fully constrained, and Parks Size is an operational ordinal classification rather than a direct measurement of avalanche mass, volume or kinetic energy. The adopted correction accounts for the changing 3-D source-to-array distance but does not explicitly include complex topographic or atmospheric propagation effects.

Future work will extend the analysis to the full ADN dataset, comprising thousands of detected avalanches since 2018, to assess the robustness of the observed IAVE–Size relationship across different paths, terrain configurations and propagation conditions. Combining this larger statistical analysis with detailed multi-sensor observations will also be essential to better constrain the infrasonic source mechanism and determine whether IAVE can ultimately be related quantitatively to avalanche mass, kinetic energy, or other physically meaningful measures of avalanche magnitude.

REFERENCES

Canadian Avalanche Association (2024). Observation Guidelines and Recording Standards for Weather, Snowpack and Avalanches, 2024 Edition. Canadian Avalanche Association, Revelstoke, British Columbia, Canada.

Hafner, E. D., Techel, F., Daudt, R. C., Wegner, J. D., Schindler, K., and Bühler, Y. (2023). Avalanche size estimation and avalanche outline determination by experts: reliability and implications for practice. Natural Hazards and Earth System Sciences, 23, 2895–2914. https://doi.org/10.5194/nhess-23-2895-2023.

Hendrikx, J., Dreier, L., Ulivieri, G., Sanderson, J., Jones, A., Steinkogler, W. (2018). Evaluation of an infrasound detection system for avalanches in Rogers Pass, Canada. In: Fischer, J.-T. (Ed.), Proceedings ISSW 2018. International Snow Science Workshop, Innsbruck, Austria, pp. 171–175, 7–12 October 2018.

Johnson, J. B., Anderson, J. F., Marshall, H. P., Havens, S., & Watson, L. M. (2021). Snow avalanche detection and source constraints made using a networked array of infrasound sensors. Journal of Geophysical Research: Earth Surface, 126(3), e2020JF005741. https://doi.org/10.1029/2020JF005741.

Mayer, S., van Herwijnen, A., Ulivieri, G., & Schweizer, J. (2020). Evaluating the performance of an operational infrasound avalanche detection system at three locations in the Swiss Alps during two winter seasons. Cold Regions Science and Technology, 173, 102962. https://doi.org/10.1016/j.coldregions.2019.102962

McClung, D. M., and Schaerer, P. A. (1981). Snow avalanche size classification. In: Proceedings of an Avalanche Workshop, Vancouver, BC, Canada, 3–5 November 1980, pp. 12–27. National Research Council of Canada, Associate Committee on Geotechnical Research, Technical Memorandum 133.

Sovilla, B., Marchetti, E., Kyburz, M.L., Köhler, A., Hguenin, P., Calic, I. (2025). The Dominant source mechanism of infrasound generation in powder snow avalanches. Geophysical Research Letters, 52, e2024GL112886. https://doi.org/10.1029/2024GL112886.

Ulivieri, G., Marchetti, E., Ripepe, M., Chiambretti, I., De Rosa, G., and Segor, V. (2011). Monitoring snow avalanches in Northwestern Italian Alps using an infrasound array, Cold Reg. Sci. Technol., 69, 177–183, https://doi.org/10.1016/j.coldregions.2011.09.006.